REVIEWED

Lattice Boltzmann Simulation of Multiple Droplet Interaction on Non-ideal Surfaces for Inkjet Deposition

Wenchao Zhou
The AM^3 Lab, Department of Mechanical Engineering, University of Arkansas at Fayetteville
Fayetteville, AR, United States of America; email: zhouw@uark.edu

Abstract

Inkjet deposition enables a more efficient, economic, scalable manufacturing process for a wider variety of materials than other traditional additive techniques. The interaction dynamics of inkjettted droplets on surfaces are crucial for controlling the formation of the printed patterns, the accuracy of which is critical to the functionalities of the printed device (e.g., electronics). However, little research has been reported on this front due to the prohibitive computational cost of simulating the dynamics of multiple droplet interaction on surfaces. Recently, Zhou et al. [1] reported an efficient numerical solver based on Lattice Boltzmann Method (LBM) that enabled the simulation of multiple droplet interaction dynamics on an ideal surface (i.e., smooth and homogeneous). In this model, the final shape of the droplets always relax back to the equilibrium shape (i.e., spherical cap) prescribed by the static contact angle of the idea surface, which does not provide any useful information on the final printed pattern. In order to simulate the printed pattern in real world, it is necessary to take into consideration of the contact angle hysteresis phenomenon on a non-ideal surface, which is caused by the surface roughness and chemical inhomogeneity of the surface. In this paper, a dynamic contact angle boundary condition is developed to take into account the contact angle hysteresis effect based on the previously reported LBM model. The improved LBM model was validated with experimental data from literature. The influence of the printing conditions, droplet spacing, and surface conditions on the two-droplet interaction dynamics were investigated with the validated LBM model. Interesting phenomena were observed and discussed. The interaction of a line of six droplets on a non-ideal surface was simulated to demonstrate the powerful capability of the developed numerical solver in simulating real-world inkjet printing process.

Introduction

As a digital material distribution technology, inkjet has become an increasingly popular choice for manufacturing, such as printed electronics and printing 3D structures. The interaction dynamics between the droplets and the substrate are critical to the accuracy and quality of the printed pattern, especially for electronics printing, where inaccuracy may lead to malfunction of the circuits (e.g., shorting or breaking). Droplet impinging on a substrate is a century-old problem that involves physics spanning multiple length scales, from Van der Waals force to capillary length. A standard no-slip wall boundary would not apply to a moving contact line. A full understanding of the contact line dynamics is still elusive [2]. Nonetheless, significant research progresses have been reported over the past century, including experimental observations [3-6], analytical modeling [7-10], and numerical simulations [11-15]. Most of prior research focused on the spreading dynamics of single droplet on a substrate due to the difficulty of conducting experiments on multiple droplet interaction and the prohibitive computational cost for simulating multiple droplet interaction dynamics.

Understanding of multiple droplet interaction dynamics is important to understand inkjet deposition as a manufacturing process. Zhou et al. [1] developed an efficient numerical

algorithm based on the Lattice Boltzmann (LB) method that is capable of simulating multiple droplet interaction dynamics on a solid substrate ~100 times faster than conventional commercial software. Their research demonstrated that multiple droplet interaction dynamics is much more complex than single droplet impingement dynamics, which are not only influenced by the impingement velocity and fluid properties, but also further complicated by the droplet spacing and the number of droplets. In their model, however, an ideal smooth and homogeneous surface was used, which could not be used to simulate real-world inkjet deposition process because droplets behave differently on a real surface than on an ideal surface.

Contact angle hysteresis, a phenomenon referred to the difference between the advancing contact angle and the receding contact angle for a contact line moving in opposite direction at the same velocity on a surface, often occurs on real surfaces due to surface roughness and chemical inhomogeneity. Without contact angle hysteresis, the droplets would coalesce into a large droplet sitting on the surface, which would make it difficult to print a line or other feature patterns using inkjet. Therefore, in order to simulate inkjet deposition process, it is important to take into account contact angle hysteresis. Similar to the contact line dynamics, research on the theory of contact angle hysteresis is far from settled despite decades of research efforts have been devoted to it [16, 17]. From a perspective of free energy, one explanation is that there exists a local minimum in Gibbs free energy of the droplet between the advancing contact angle and the receding contact angle and a contact angle larger than the advancing contact angle or smaller than the receding contact angle is required to overcome this local energy barrier [18]. Extensive research has also been reported on the numerical modeling of contact angle hysteresis. P. Spelt developed a level-set approach for simulations of flows with multiple moving contact lines with hysteresis [19]. Wang et al. developed a multiphase LB scheme for simulating the dynamic behavior of a droplet sliding along a wall with contact angle hysteresis [20]. Kusumaatmaja et al. also developed a LB model to simulate droplet behavior with contact angle hysteresis on chemically patterned and superhydrophoboic surfaces [21].

However, none of the previous research has studied multiple droplet interaction dynamics on a real surface with contact angle hysteresis, the understanding of which is critical to improve the printing accuracy and quality of inkjet. In this paper, an efficient LB model is developed for simulating multiple droplet interaction on a real surface based on the model in [1]. The LB model is then validated against experimental data from literature [22]. Simulations are performed with the validated numerical model to study two-droplet interaction under various conditions with an objective of forming a uniform line on the substrate. Simulations of a line of six droplets interacting with each other are also conducted to demonstrate the powerful capability of the developed numerical solver in simulating real-world inkjet deposition process. Results show the multiple droplet interaction dynamics in inkjet deposition process is much more complex than the single droplet impingement dynamics examined by previous research. This paper provides the first peek into this complex dynamics and discusses some interesting phenomena observed. The rest of the paper is organized as follows. In section 2, the proposed LB model with contact angle hysteresis is presented and validated. Results obtained from simulations with the validated LB model are discussed in section 3. Conclusions are given in section 4.

Lattice Boltzmann Modeling

A. Lattice Boltzmann method for two-phase flows

The multiphase LB model used here was originally proposed by He et al. [23] and improved by Zhou et al. [1]. Two distribution functions were used to track the evolution of the pressure field and the phase composition of the fluid:

$$\frac{\partial g_i}{\partial t} + \mathbf{e}_i \cdot \nabla g_i = -\frac{g_i - g_i^{(0)}}{\lambda} + (\mathbf{e}_i - \mathbf{u}) \cdot [\Gamma_i(\mathbf{u}) \cdot \mathbf{F} + \Gamma_i(0) \cdot \nabla\psi(\rho)] \quad (1)$$

$$\frac{\partial h_i}{\partial t} + \mathbf{e}_i \cdot \nabla h_i = -\frac{h_i - h_i^{(0)}}{\lambda} + (\mathbf{e}_i - \mathbf{u}) \cdot \left(\frac{C}{\rho c_s^2}\mathbf{F} + \nabla C - \frac{C}{\rho}\nabla\rho\right)\Gamma_i(\mathbf{u}) + \Gamma_i(\mathbf{u})\nabla \cdot M\nabla\mu \quad (2)$$

where $g_i \equiv g_i(\boldsymbol{x}, \mathbf{e}_i, t)$ and $h_i \equiv h_i(\boldsymbol{x}, \mathbf{e}_i, t)$ are the distribution functions for tracking the evolution of pressure field and phase composition C respectively, $\boldsymbol{x}$ is the spatial coordinates, $\mathbf{e}_i$ is the local particle velocity in the i^{th} direction of a discretized velocity space, λ is the time scale for local particle distribution relaxing back to its equilibrium state, $\mathbf{F}$ is the external body force exerted on a particle, ρ is fluid density, c_s is the lattice speed of sound, which is a scaling factor that depends on the specific lattice structure [24], $\mathbf{u}$ is the macroscopic velocity of fluid, M is mobility, μ is chemical potential, $g_i^{(0)}$ and $h_i^{(0)}$ are the equilibrium distribution functions, and

$$\Gamma_i(\mathbf{u}) = t_i\left[1 + \frac{\mathbf{e}_i \cdot \mathbf{u}}{c_s^2} + \frac{(\mathbf{e}_i \cdot \mathbf{u})^2}{2c_s^4} - \frac{\mathbf{u} \cdot \mathbf{u}}{2c_s^2}\right];\ \psi(\rho) = p - \rho c_s^2 \quad (3)$$

$$p = \sum g_i\ ;\ \rho\mathbf{u}c_s^2 = \sum g_i\mathbf{e}_i \quad (4)$$

$$\sum g_i^{(0)} = p;\ \sum g_i^{(0)}\mathbf{e}_i = \rho\mathbf{u}c_s^2 \quad (5)$$

$$\sum h_i = C;\ \sum h_i\mathbf{e}_i = C\mathbf{u} \quad (6)$$

$$\sum h_i^{(0)} = C;\ \sum h_i^{(0)}\mathbf{e}_i = C\mathbf{u} \quad (7)$$

where p is pressure, t_i is the weighting factor that depends on the specific lattice model, which is usually identified as *d*-dimensional *b*-velocity *DdQb* model. A summary of different lattice models can be found in [25].

A diffusive interface model is employed, in which the moving contact line is driven by the chemical potential gradient to minimize the Gibbs free energy in the droplet. This resolves the singularity issue caused by the no-slip wall boundary condition. This is realized by defining the interaction force between the fluid particles $\mathbf{F}$ in a way such that the LB equations can recover the macroscopic phase-field equations:

$$\mathbf{F} = -\nabla\psi(\rho) + \mu\nabla C + \rho\mathbf{g} \quad (8)$$

where μ is the chemical potential defined as derivative of Gibbs free energy with respect to C at constant temperature and pressure:

$$\mu = 4\beta(C - C_l)(C - (C_l + C_h)/2)(C - C_h) + \kappa\nabla^2 C \quad (9)$$

where β is a constant relating to bulk free energy, C_l and C_h equal to 0 and 1 respectively, representing two different phases (i.e., liquid and surrounding air), and κ is a parameter related to surface tension σ.

B. Contact angle hysteresis

When a liquid droplet is sitting on a solid surface, a static contact angle θ_s, which can be determined by the famous Young's equation, is typically used to characterize the wetting behavior of the liquid on the surface. In reality, the observed contact angles are usually not equal to θ_s on a non-ideal surface. There exist many metastable states of a droplet on a solid, possibly due to surface roughness or chemical inhomogeneity of the surface. When the contact angle is

increased to a certain extent, the metastable state will no long hold and the droplet will start expanding (or advancing) on the substrate. This contact angle is often referred as the advancing contact angle θ_a. On the other hand, if the contact angle is decreased to a certain value, the droplet will start contracting (or receding) on the substrate. This contact angle is referred as the receding contact angle θ_r. The difference between the advancing and receding contact angles is called the contact angle hysteresis H:

$$H = \theta_a - \theta_r \tag{10}$$

The contact angle hysteresis for a solid surface can be experimentally measured using various methods, such as direct measurement by telescope-goniometer [26], tilting plate method [27], and the Wilhelmy balance method [28].

To implement the wetting boundary conditions for an ideal solid surface described by a static contact angle θ_s, most of previous research adopted a surface energy formulation by taking into account the wall free energy through linear, quadratic, or cubic approximations [29, 30]. Recent studies found a geometric formulation is computationally more efficient and accurate than the surface energy formulation [1, 31]. In this paper, we expand the geometric formulation to model the contact angle hysteresis. The geometric relationships are illustrated in Figure 1. In a static or quasi-static situation, if the current contact angle is larger than the advancing contact angle θ_a, the contact line shall advance to reduce the contact angle in an attempt to bring the droplet back to the metastable state. If the current contact angle is smaller than the receding the receding contact angle θ_r, the contact line shall recede. If the current contact angle θ is in between of the advancing contact angle θ_a and the receding contact angle θ_r, the contact line shall remain pinned and the contact angle shall remain unchanged. In light of this analysis, the wetting boundary condition for contact angle hysteresis is formulated as follows. At each time step during the simulation, the current contact angle is first determined using the following relationship:

$$\cos(\theta_c) = \frac{\mathbf{n} \cdot \nabla C}{|\nabla C|} \tag{11}$$

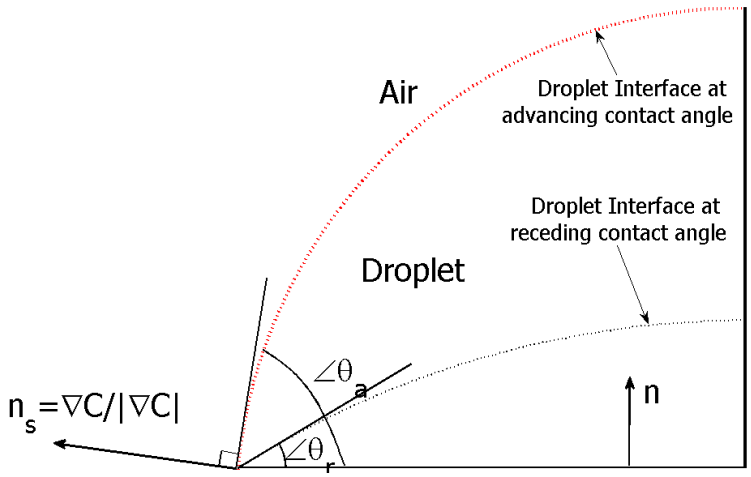

Figure 1. Illustration of the geometric relationships of the advancing and receding contact angles

The following boundary condition will then be applied at every time step:

$$\tan\left(\frac{\pi}{2} - \theta\right) = \frac{\mathbf{n} \cdot \nabla C}{|\nabla C - (\mathbf{n} \cdot \nabla C)\mathbf{n}|} \tag{12}$$

where $\theta = \theta_c$ if $\theta_r < \theta_c < \theta_a$, and $\theta = \theta_r$ if $\theta_c < \theta_r$, and $\theta = \theta_a$ if $\theta_c > \theta_a$.
This boundary condition enforces contact angle hysteresis effect on the surface, whether it is caused by surface roughness of chemical inhomogeneity.

C. Validation

We implemented a numerical solver based on the proposed LB scheme and wetting boundary condition with contact angle hysteresis. The numerical model was validated against the experimental data obtained from S. Sikalo et al. [22] by simulating a single droplet impinging on a non-ideal surface under the same conditions with the experiments. Two sets of experimental data were selected. The liquid used was a mixture of water and glycerin with a density of 1220 kg/m^3, a surface tension of 0.063 N/m, and a viscosity of 116 mPa*s. The droplet size was 2.45 mm and a wax surface was used as the substrate with an advancing contact angle of 97˚ and a receding contact angle of 90˚. The impact velocities for the two experiments were 1.41 m/s and 1.04 m/s respectively, resulting in a Weber number of 93 and 51 respectively. Simulations were performed with the LB solver and the change of the spread factor D* (defined as the ratio of the diameter of the wetting area D to the droplet diameter D_0) over time were compared. The results comparison are shown in Figure 2. We can see that overall there is a good agreement between the experiment and the simulation results. Since the proposed LB model is for solving the governing equations for the multiphase flow dynamics, it is appropriate to use this validated model to study multiple droplet interaction dynamics although the validation is based on single droplet dynamics, because the governing equations for single droplet and multiple droplet dynamics are the same.

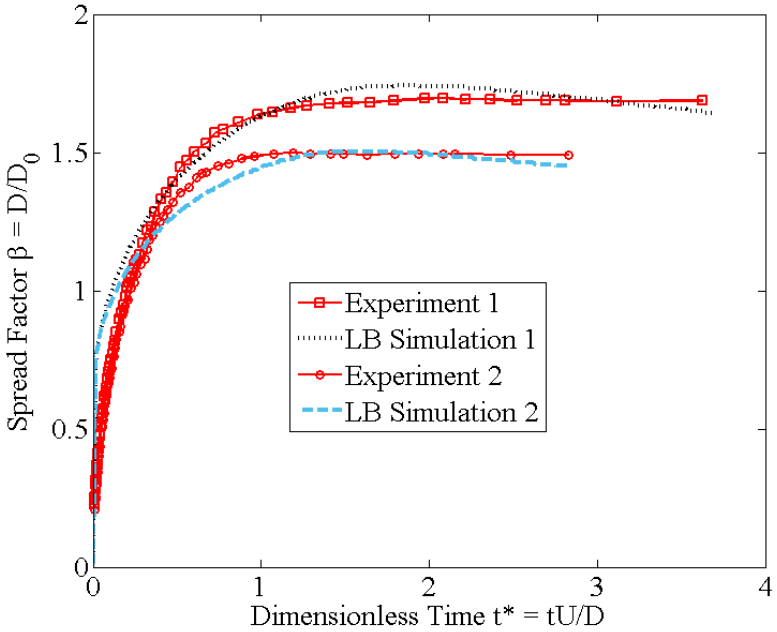

Figure 2. Validation of the LB solver against the experimental data from S. Sikalo et al. [22]. Experiment 1: impact velocity 1.41 m/s; Weber number 93; Reynolds number 36. Experiment 2: impact velocity 1.04 m/s; Weber number 51; Reynolds number 27.

Results and Discussion

Without a non-ideal surface, it would be impossible to use inkjet for printing patterns because all the droplets will coalesce into a big droplet on an ideal surface and come to the equilibrium

shape that is only dictated by the static contact angle and gravity. On the other hand, a non-ideal surface will have complex interaction with the droplets and the final printed pattern will not only be influenced by the surface conditions, but also by the interaction dynamics (i.e., the evolution of the shape of the droplets) that are also impacted by the printing conditions (e.g., droplet size, ink properties, and impingement velocity) and the droplet spacing. Simulation of such complex interaction dynamics is now made possible with the numerical model developed in this paper, which affords us a digital tool to study how the printing and surface conditions will affect the final outcome of the printed pattern.

One of the particular interests is to print a straight line (e.g., for conductive paths in electronics). In order to obtain insights into the complex dynamics, we start from the simplest case, two droplet interaction. In this section, we will investigate the effects of the printing conditions, droplet spacing, and surface conditions with simulations. And we will also demonstrate the powerful capability of the developed numerical solver in simulating the process of printing a line of six droplets.

A. Effects of printing conditions on two-droplet interaction

Printing conditions include the impingement velocity of the droplet U, the fluid properties (e.g., surface tension σ, viscosity μ, and density ρ), and the droplet diameter D_0. From previous research [15, 32], the printing conditions can be characterized by two dimensionless numbers: Weber number ($We = \rho U^2 D_0/\sigma$) and Ohnesorge number ($Oh = \mu/\sqrt{\rho\sigma D_0}$). These two dimensionless numbers divide the droplet interaction dynamics into four different regimes characterized by the driving and resisting forces shown in Table 1.

Table 1. Four different regimes for characterizing the printing conditions

	Oh < 1 (almost inviscid)	Oh > 1 (highly viscous)
We > 1 (inertia driven)	Regime I (driven by inertia, resisted by surface tension)	Regime IV (driven by inertia, resisted by viscosity)
We < 1 (surface tension driven)	Regime II (driven by surface tension, resisted by inertia)	Regime III (driven by surface tension, resisted by viscosity)

Simulations for two-droplet interaction dynamics were performed with the developed numerical solver. The droplet spacing (defined as the ratio of initial distance between the centroids of the two droplets to the droplet diameter) is set to be 1.3. The advancing and receding contact angles are set to be 120˚ and 60˚ respectively. Because of our interests in knowing how well the contact angle hysteresis effect can keep the droplets stick to the locations on the surface where they are deposited to prevent the surface tension from pulling them into a big droplet and thus form the designed print pattern, two metrics were used to study the interaction dynamics. The two metrics are footprint length and width and their definition is illustrated in Figure 3.

The evolution of the footprint length and width over time in the four regimes are shown in Figure 4 to Figure 7 along with the snapshots of the droplet interaction at different time instants. In regime I, the Weber and Ohnesorge numbers are set to be 100 and 0.04 respectively. Therefore, the inertia is dominating and viscous dissipation is small (i.e., high impingement velocity and low viscosity). As shown in Figure 4, the droplets initially spread in both the x and y direction (shown in Figure 3). The footprint length is larger because the two droplets are initially separated

at a distance in the x direction. The inertia drives the spreading of the droplets until they meet. The timing of the meeting, mainly influenced by droplet spacing under the same printing conditions, has profound impact on the evolution of the droplets interaction for two reasons. One is the timing determines how much kinetic energy the droplets have before the meeting. The other is the coalescence of the droplets will lead to a sudden release of interface energy, which would be converted into kinetic energy. This sudden local change of energy around the meeting location will change the rest of the evolution. In this case, as can be seen from Figure 4, after the droplets changed from spreading to receding at the first peak (footprint width), the liquid at the meeting location, gained extra kinetic energy from the coalescence of the interface, kept spreading, and led to the second peak for the footprint width. The first peak and the second peak occur at different locations as shown at t* = 3.36 (near the centroids of the droplets) and t* = 6.72 (near the meeting location). As the droplets kept deforming, the kinetic energy was converted to surface energy and dissipated during the process. The surface energy was then converted back to kinetic energy, leading to the receding of the droplets. One observation was that the droplets were receding in the x direction while they were advancing in the y direction. One possible explanation is that, because of the asymmetry in x and y direction, the surface is more deformed in the x direction and therefore faces more "pressure" to recede as surface tension prefers a minimum surface. After the coalescence of the droplets, if the leftover kinetic energy is small, not enough to overcome the energy barrier imposed by the receding contact angle, the droplets would come to equilibrium on the substrate at a contact angle larger than the receding contact angle in the x direction and a contact angle smaller than the advancing contact angle in the y direction, and maintain an elongated "line" as desired. However, if the leftover kinetic energy is sufficiently large, which is the case for the simulation in Figure 4, the droplets will recede in the x direction and eventually relax back to a single droplet sitting on the substrate at the contact angle equal to or larger than the receding contact angle, as shown in Figure 4. This will not the ideal printing condition for printing a line as the final length to width ratio is close to 1.

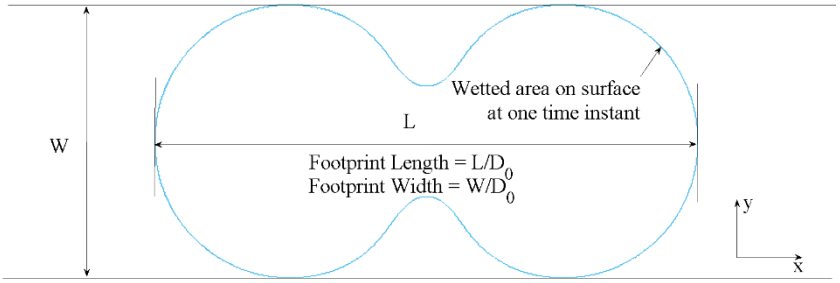

Figure 3. Illustration of the definition of footprint length and width: defined as the ratios of the distance between two furthest points along x and y direction to the droplet diameter. The contour is the cross section of the wetted area (i.e. the footprint) of the droplets on the substrate at one time instant.

In regime II, the Weber and Ohnesorge numbers are set to be 0.01 and 0.04 respectively. This is a regime driven by surface tension and resisted by inertia (i.e., low impingement velocity and low viscosity). Viscous force plays very little role. The surface tension drives the spreading of the droplets in both x and y direction before they meet. Because surface tension is the dominating force, a clear "hiccup" occurs when the droplets meet at approximately the time t* = 1 as shown in Figure 5. The meeting leads to a contraction in both the x and y directions due to the sudden increase of energy pulling the liquid towards the meeting point. Then the droplets start to recede in the x direction and spread in the y direction. Due to the contact angle hysteresis

effect, the droplets deforms to reduce the contact angle to become smaller than the receding contact angle so it can recede (see t* = 1.01 and t* = 1.18 in Figure 5). Because the kinetic energy is small, the liquid will stop receding in the x direction once it reaches a metastable state (i.e., contact angle slightly larger than or equal to the receding contact angle), and stop advancing in the y direction once the contact angle becomes smaller than the advancing contact angle. From this analysis, it can be seen that the final shape of the droplets will be primarily determined by the advancing and receding contact angles although the evolution history still plays a role. This printing condition does produce an elongated "line" as desired and the length to width ratio is 1.55.

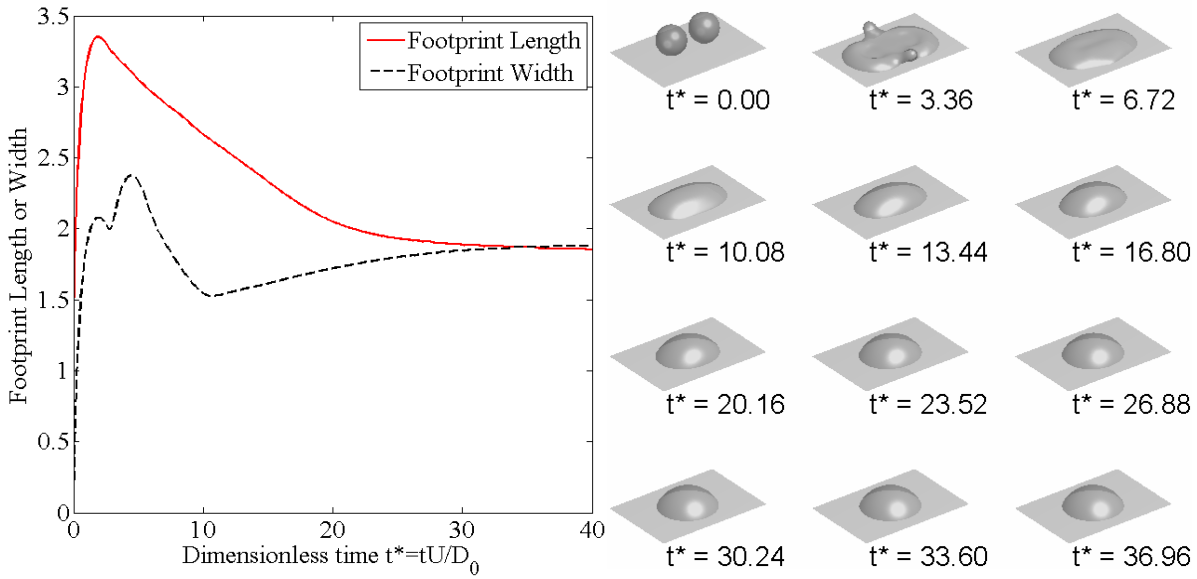

Figure 4. Regime I (We = 100; Oh = 0.04): evolution of footprint length and width over time for two droplet interaction in regime I along with their snapshots at different time instants. t is dimensionless time.*

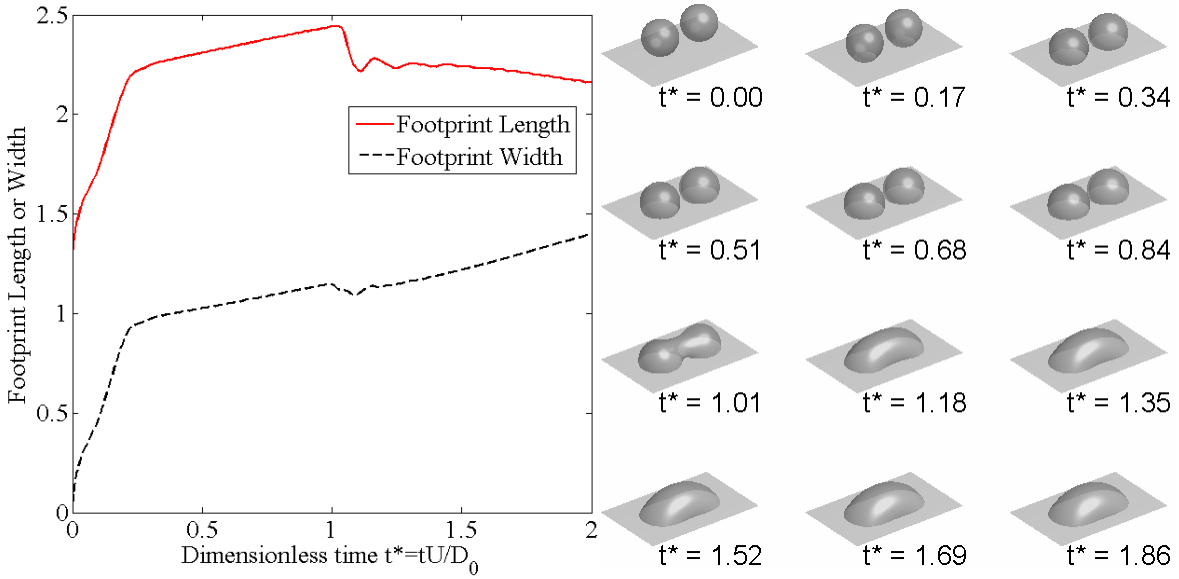

Figure 5. Regime II (We = 0.01; Oh = 0.04): evolution of footprint length and width over time for two droplet interaction in regime II along with their snapshots at different time instants. t is dimensionless time.*

In regime III, the Weber and Ohnesorge numbers are set to be 0.25 and 4 respectively. In this regime, the viscous force is dominating (i.e., low impingement velocity and high viscosity). As shown in Figure 6, after initial spreading upon contact with the substrate, the droplets are dominated over by the viscous force and spread at a very slow rate. The meeting of the two droplets spurs a quick receding in the x direction. Because the viscous dissipation is so high, there is not enough kinetic energy to overcome the energy barrier to advance or recede on the substrate. Driven by surface tension, the droplets achieve different metastable states in x and y directions due the asymmetry. The final footprint length to width ratio obtained from the simulation is 1.24.

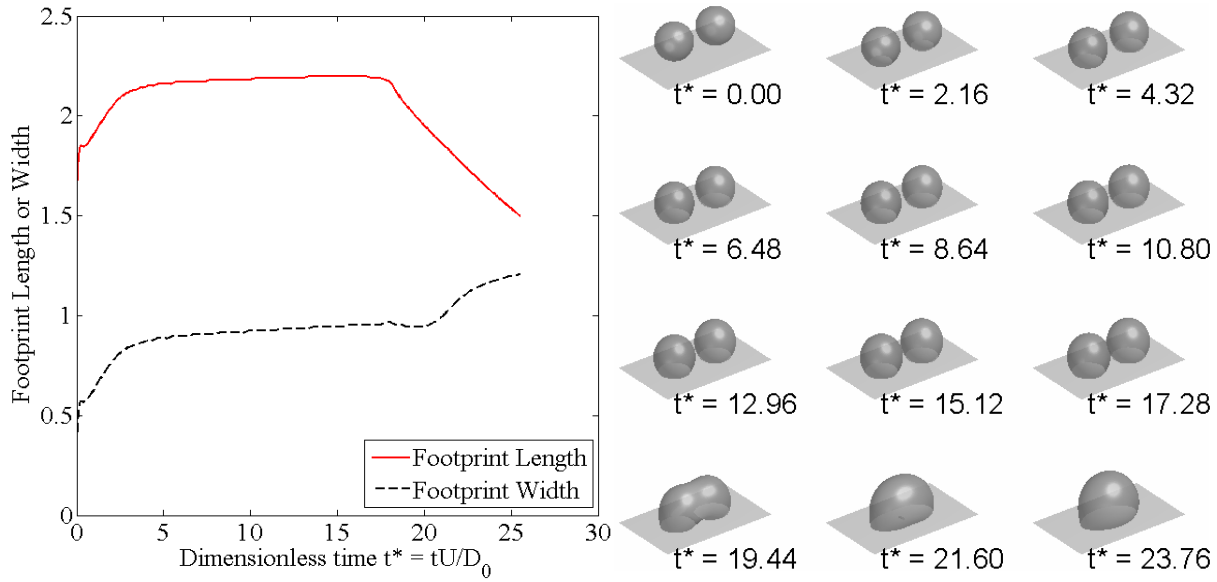

Figure 6. Regime III (We = 0.25; Oh = 4): evolution of footprint length and width over time for two droplet interaction in regime III along with their snapshots at different time instants. t is dimensionless time.*

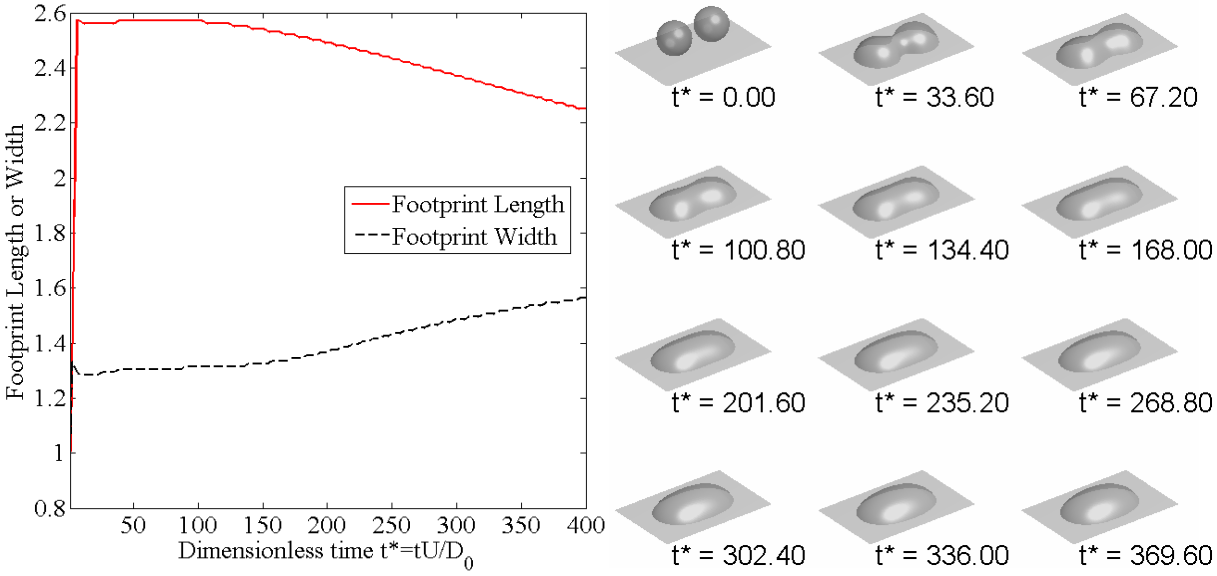

Figure 7. Regime IV (We = 400; Oh = 4): evolution of footprint length and width over time for two droplet interaction in regime IV along with their snapshots at different time instants. t is dimensionless time.*

In Regime IV, the Weber and Ohnesorge numbers are 400 and 4 respectively. This regime has high impingement velocity and high viscosity. The results are shown in Figure 7. In the beginning stage, the droplets are "bombarded" onto the substrate at a very high velocity and they deform quickly as shown in Figure 7 (i.e., a sharp increase in footprint length and width). In this regime, the timescale of the inertial force is shorter than that of the viscous force, which is shorter than that of surface tension. Therefore, after the large deformation driven by the inertial force during the short timespan in the beginning stage, the viscous force kicks in and slows everything down. The footprint doesn't change much during this stage, even though the meeting of the two droplets during this stage doesn't cause any obvious change, because viscous force is dominating. In later stage at a longer time scale, the surface tension starts to drive the motion of the droplets. Similar to regime III, surface tension becomes the primary driving force and most of the kinetic energy is dissipated by the high viscosity. Therefore, the droplets will enter metastable states in between the advancing contact angle and receding contact angle based on the energy evolution history. Due to asymmetry, the metastable states are different in the x direction from in the y direction as the droplets are receding in the x direction and advancing in y direction. In this case, the final length to width ratio is 1.44, which is in an elongated "line".

B. Effects of droplet spacing and surface conditions on two-droplet interaction

Other than the printing conditions, the droplet spacing and surface conditions (i.e., the advancing and receding contact angles) also play significant role in determining the outcome of the droplet interaction dynamics. Because most of the inkjet printers operate in regime I (i.e., high impingement velocity and low viscosity), we have performed simulations with the validated numerical model in regime I with different droplet spacing and surface conditions. The Weber and Ohnesorge numbers are set to be 100 and 0.04 respectively, the same as in previous section. The receding contact angle is fixed at 30˚. The advancing contact angle is varied such that the contact angle hysteresis H (defined in Eq. (10)) varies from 10˚ to 90˚. The droplet spacing is set to 1.6 and 2. A total of 8 simulations were performed with different combinations of contact angle hysteresis and droplet spacing. The evolutions of footprint length and width over time are plotted in Figure 8 and the snapshots of 4 of these simulations are shown in Figure 9.

The first observation is that the results are very different from Figure 4, where the footprint length is almost equal to the footprint width. In Figure 8, however, we can see that the footprint lengths are larger than footprint width, leaving desirable elongated "lines". This is a result of the surface conditions. Because of the small receding angle, it becomes more difficult for the droplets to recede. Since the droplets spread further in x direction due to the asymmetric geometry, the final footprint is longer in the x direction than in the y direction. The ratios of the footprint length to width are not the same, however. They depend on the evolution dynamics. The final footprint length to width ratios for the 4 simulations in Figure 9 are 1.63, 1.45, 2.19, and 2.06 for cases a, b, c, and d, respectively. Generally, a larger droplet spacing will lead to a larger footprint length to width ratio.

The second surprising observation is that the footprint length to width ratio decreases with larger contact angle hysteresis. This result is very counter intuitive because the intuitive sense is that we would get a larger difference in x and y direction as contact angle hysteresis increases. It should be noted, however, this observation is not generally true. As will be shown later in the paper, under different conditions, a larger hysteresis would lead to a larger difference between the

footprint length and width. By carefully watching the evolution dynamics of these simulations, we believe the reason is as following. When the droplets meet, the interface coalesces and starts to advance on the surface in the y direction at the meeting location. Since receding contact angle is fixed, a larger hysteresis means a larger advancing contact angle, which would make it more difficult for the droplets to advance in the y direction. As a result, it creates an extra pull in the x direction, causing the droplets to recede faster in the x direction.

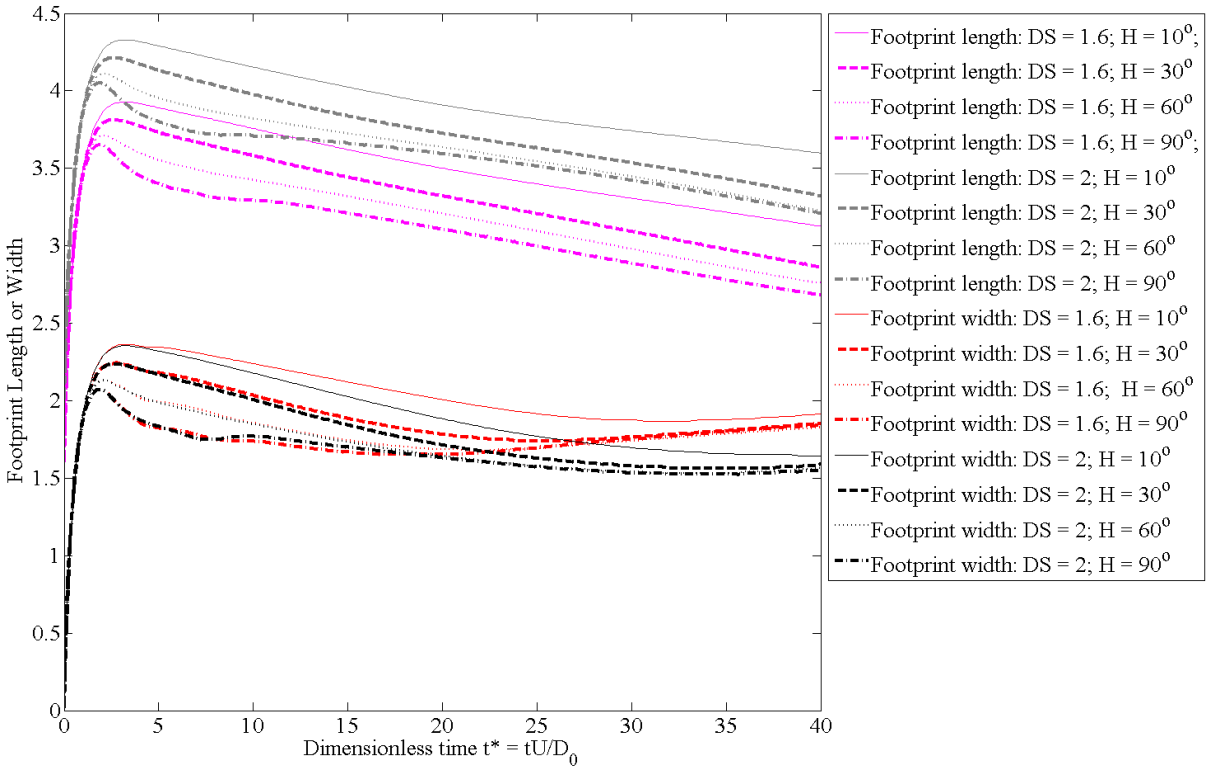

Figure 8. Evolution of footprint length and width over time in regime I (We = 100; Oh = 0.04) at different droplet spacing (DS) and contact angle hysteresis H (defined in Eq. (10)). The receding contact angle is fixed at 30˚.

The third observation is also very surprising. As shown in Figure 8, the footprint width converges to the same value for the simulations with the same droplet spacing regardless of the contact angles. Normally for an ideal surface, the footprint would be the same for the same contact angle. We believe one of the necessary conditions for this result is that the receding contact angle needs to be the same. As will be shown later in the paper, when the receding contact angles are not the same, the footprint width will not be the same even with the same droplet spacing and the same contact angle hysteresis. It seems receding contact angle plays a more important role than the advancing contact angle in influencing the interaction dynamics.

In order to compare and get a better understanding of the influence of the droplet spacing and surface conditions, simulations with the exact same conditions (i.e., We = 100; Oh = 4; H = 30˚ and 90˚; DS = 1.6 and 2) were performed. The only difference is instead of fixing the receding contact angle at 30˚, the advancing and receding contact angles are chosen such that their average is 90˚. The results are plotted in Figure 10. As can be seen, two of the cases for contact angle hysteresis of 30˚ did not produce a desirable elongated "line" (i.e., footprint length is almost equal to footprint width). When the contact angle hysteresis becomes 90˚, an elongated "line" is produced. The ratio of footprint length to width increases with larger contact angle

hysteresis, which is opposite to the results in Figure 8. In addition, for the same droplet spacing, the footprint width doesn't converge, which is also different from Figure 8. From these simulations, it becomes clear that the receding contact angle plays a more important role than the contact angle hysteresis H in influencing the final footprint length to width ratio.

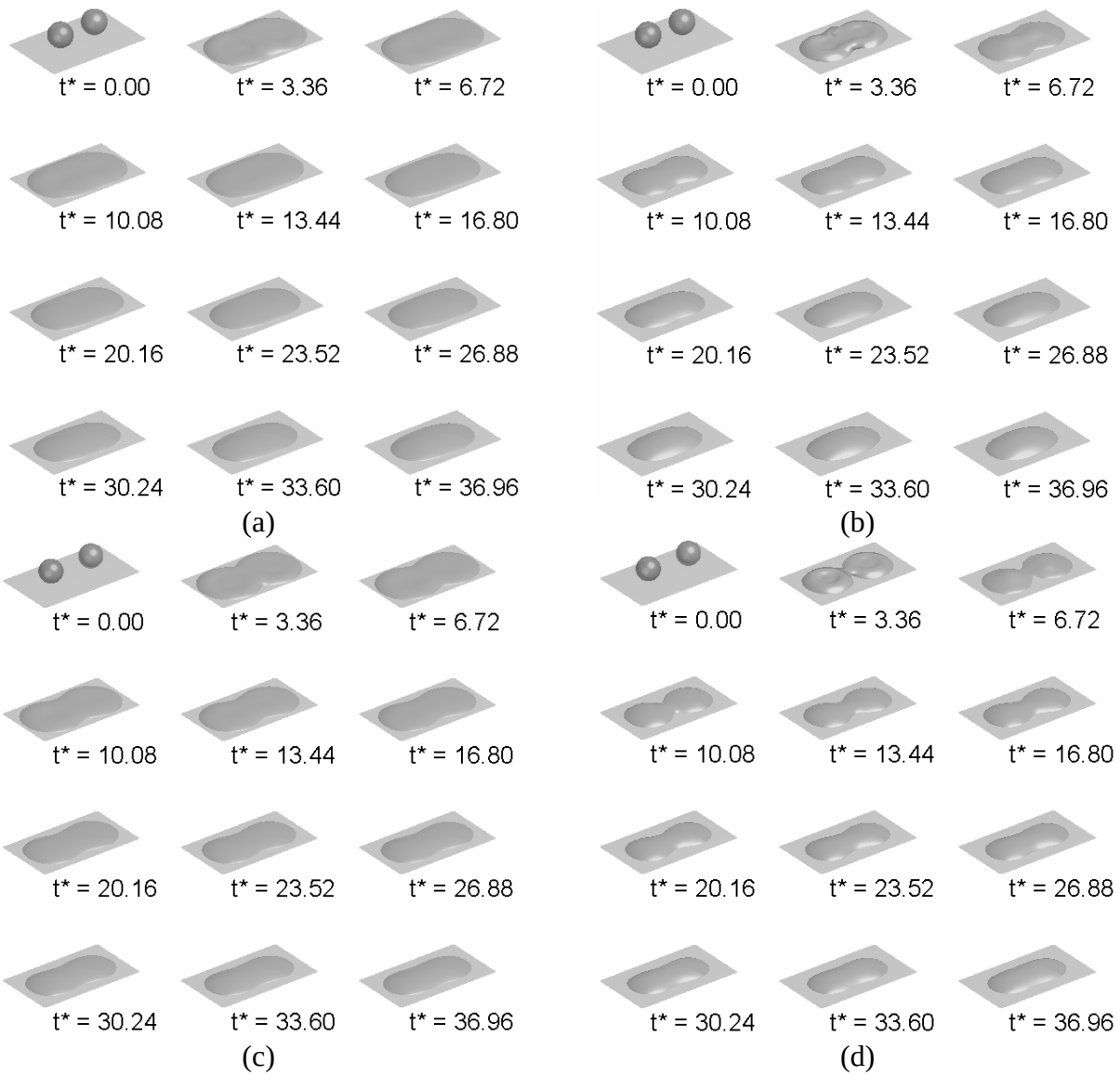

Figure 9. Snapshots of two-droplet interaction over time in regime I (We = 100; Oh = 0.04) at different droplet spacing (DS) and contact angle hysteresis H (defined in Eq. (10)). The receding contact angle is fixed at 30°. (a). DS = 1.6; H = 10°; the final footprint length to width ratio is 1.63; (b). DS = 1.6; H = 90°; the final footprint length to width ratio is 1.45; (c). DS = 2; H = 10°; the final footprint length to width ratio is 2.19; (d). DS = 2; H = 90°; the final footprint length to width ratio is 2.06.

C. Six-droplet interaction

As the number of droplets increases, the interaction dynamics will become more complex and thus more difficult to predict, which could significantly compromise the much needed accuracy and precision for manufacturing with inkjet. Many possible negative outcomes have been reported, such as broken lines, undulating lines, and rounded squares [33]. The numerical solver developed in this paper provides us a great digital tool for simulating and predicting the outcome

of the multiple droplet interaction dynamics on real surfaces for inkjet deposition. This section presents a simulation of the interaction dynamics of 6 droplets in a line to demonstrate the powerful capability of this numerical solver. The printing condition is the same as that in regime I with a Weber number of 100 and Ohnesorge number of 0.04. The droplet spacing is set to be 1.6. The droplets are aligned sequentially in a line with the height of next droplet $0.2D_0$ higher than the previous one to mimic the condition in real inkjet process that the droplets do not land on the substrate at the same time, but one after another sequentially. The advancing and receding contact angles are set to be 150˚ and 30˚ respectively. The results are shown in Figure 11. As we can see, the coalesced droplets neck at the location where they meet due to the large contact angle hysteresis. This is because the large advancing contact angle make the coalesced interface difficult to advance in the y direction. The necking eventually leads to the liquid break into individual droplets with irregular shapes. Noticeably the two droplets on the two ends behave differently than the rest of the droplets because they only have one neighboring droplet. After breaking into individual droplet around t* = 20.40, the droplets then slowly advance on the substrate and the droplets in the middle eventually merge back together. The two droplets on the two ends, however, remain separate. This simulation shows a printed line with six droplets and the final footprint length to width ratio is 5.15. The line is not as uniform as desired, and there are two breaking points at the two ends, which are not desirable for electronics printing and could be remedied by optimizing the printing parameters. This simulation demonstrates the powerful capability of our numerical solver in simulating real-world inkjet printing process and the possibility of using this powerful digital tool for improving our understanding of and optimizing the inkjet printing process.

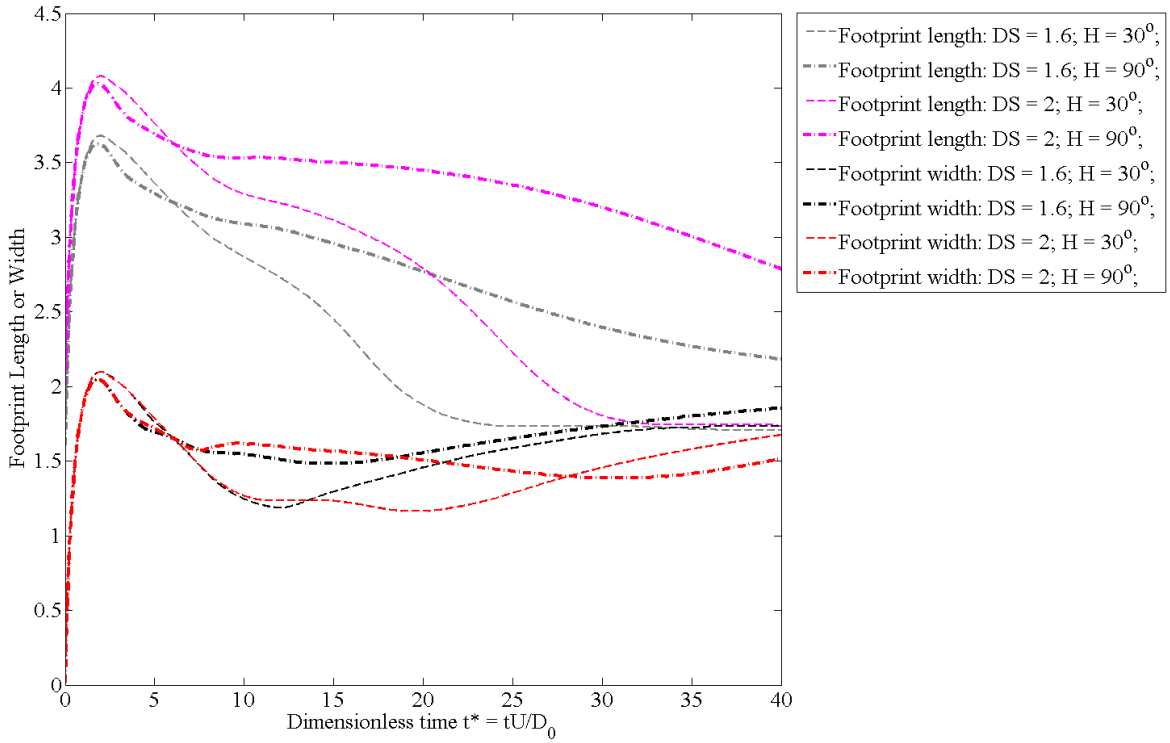

Figure 10. Evolution of footprint length and width over time in regime I (We = 100; Oh = 0.04) at different droplet spacing (DS) and contact angle hysteresis H (defined in Eq. (10)). The average of the advancing and receding contact angles is set at 90˚.

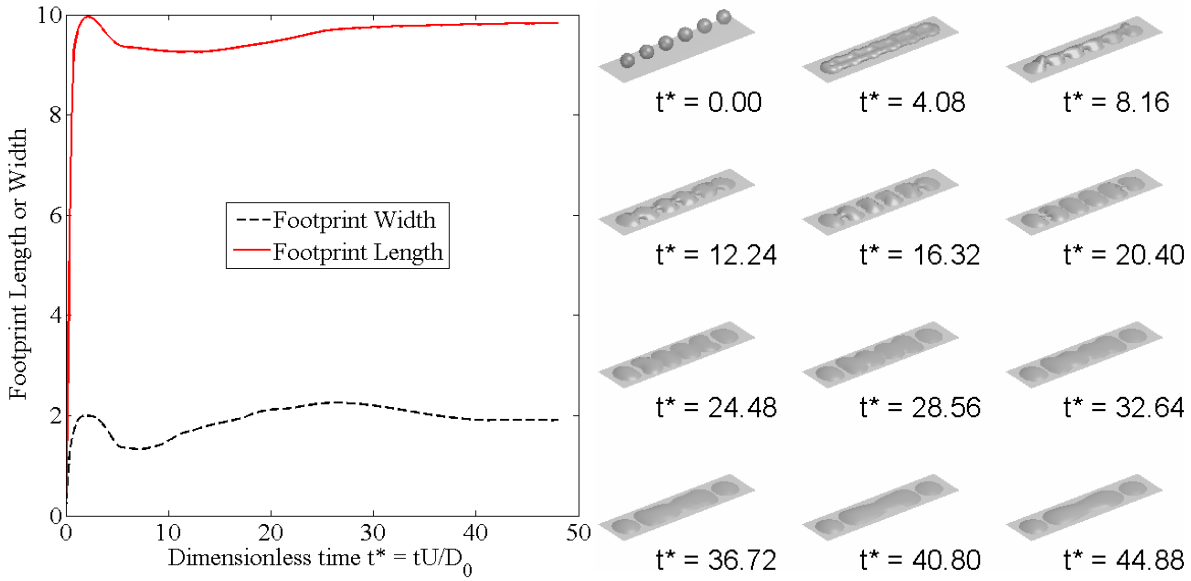

Figure 11. Six-droplet interaction in regime I (We = 100; Oh = 0.04; DS = 1.6; θ_a = 150˚; θ_r = 30˚): evolution of footprint length and width over time for two droplet interaction in regime III along with their snapshots at different time instants. t is dimensionless time.*

Conclusions

A powerful numerical model was developed based on the lattice Boltzmann method for simulating the dynamics of multiple droplet interaction on a non-ideal surface in real-world inkjet deposition process. Contact angle hysteresis effect was taken into account with a geometric wetting boundary condition. The numerical model was validated with experimental data from literature. The validated numerical model was then used to study multiple droplet interaction dynamics on a non-ideal surface. In order to understand the complex interaction dynamics, we started from the simplest case, two-droplet interaction. The two-droplet interaction dynamics were examined with an objective to print an elongated "line" under different printing conditions, droplet spacing, and surface conditions. Results show the final outcome heavily depends on the history of the dynamics because there are many metastable states in between of the advancing and receding contact angles. Drastically different results were obtained under various conditions, which revealed the rich and complex dynamics for two-droplet interaction. Simulations show the relative magnitude of the three competing forces (i.e., inertia, surface tension, and viscous force) can significantly influence the evolution history of the droplets over numerous metastable states. Theoretically speaking, there could be infinite possible final outcomes for the interaction dynamics under different conditions, which is in sharp contrast to the droplets interaction on an ideal surface that always evolve into one single final state determined by the static contact angle of the surface. This hypothesis is supported by the simulation results in this paper. One interesting and counter intuitive observation from the simulations was when the receding contact angle was fixed at 30˚, the difference between the x and y direction became larger with smaller contact angle hysteresis. Another set of simulations showed the opposite under the same conditions except the receding contact angle was not fixed. In addition, it was shown the final footprint width was independent of the contact angle hysteresis with the same droplet spacing when the receding contact angle was fixed at 30˚. The results led us to believe that the receding contact angle plays a more important role than advancing contact angle and contact angle hysteresis in determining the final footprint length to

width ratio. A small receding contact angle is preferred for producing a more elongated "line". Finally, the interaction of a line of six droplets was simulated to demonstrate the powerful capability of our numerical solver in simulating real-world inkjet printing process. Therefore, this solver can be used as a digital tool for understanding and optimizing real-world inkjet printing process.

Acknowledgements

We gratefully acknowledge the financial support from the University of Arkansas, through the startup fund provided by the Vice Provost Office for Research and Economic Development. Any opinions, findings, and conclusions or recommendations expressed in this publication are those of the authors and do not necessarily reflect the views of the University of Arkansas.

References

1. W. Zhou, D. Loney, A.G. Fedorov, F.L. Degertekin, and D.W. Rosen, *Lattice Boltzmann simulations of multiple-droplet interaction dynamics.* Physical Review E, 2014. **89**(3): p. 033311.
2. J.-B. Dupont and D. Legendre, *Numerical simulation of static and sliding drop with contact angle hysteresis.* Journal of Computational Physics, 2010. **229**(7): p. 2453-2478.
3. E.B. Dussan, *On the spreading of liquids on solid surfaces: static and dynamic contact lines.* Annual Review of Fluid Mechanics, 1979. **11**: p. 371-400.
4. Z. Zhao, D. Poulikakos, and J. Fukai, *Heat transfer and fluid dynamics during the collision of a liquid droplet on a substrate-II. Experiments.* International Journal of Heat and Mass Transfer, 1996. **39**: p. 2791-2802.
5. H.Y. Kim and J.H. Chun, *The recoiling of liquid droplets upon collision with solid surface.* Physics of Fluids, 2001. **13**: p. 643-659.
6. R. Rioboo, M. Marengo, and C. Tropea, *Time evolution of liquid drop impact onto solid, dry surfaces.* Experiments in Fluids, 2002. **33**: p. 112-124.
7. S.E. Bechtel, D.B. Bogy, and F.E. Talke, *Impact of a liquid drop against a flat surface.* IBM J. Res. Dev., 1981. **25**: p. 963.
8. S. Chandra and C.T. Avedisian. *On the collision of a droplet with a solid surface*. in *Proceedings of the Royal Society, Series A*. 1991. London.
9. G. McHale, S.M. Rowan, and M.I. Newton, *Frenkel's method and the spreading of small sperical droplets.* J. Phys. D, 1994. **27**: p. 2619.
10. T. Mao, D.C.S. Kuhn, and H. Tran, *Spread and rebound of liquid droplets upon impact on flat surfaces.* AIChE J., 1997. **43**: p. 2169.
11. N. Hatta, H. Fujimoto, and H. Takuda, *Deformation process of a water droplet impinging on a solid surface.* Journal of Heat Transfer, 1995. **117**: p. 394-401.
12. M. Bussmann, J. Mostaghimi, and S. Chandra, *On a three-dimensional volume tracking model of droplet impact.* Physics of Fluids, 1999. **11**: p. 1406-1417.
13. M. Bussmann, S. Chandra, and J. Mostaghimi, *Modeling the splash of a droplet impacting a solid surface.* Physics of Fluids, 2000. **12**: p. 3121-3132.
14. W. Zhou, D.A. Loney, A.G. Fedorov, F.L. Degertekin, and D.W. Rosen, *Droplet impingement dynamics in ink-jet deposition.* Virtual and Physical Prototyping, 2012. **7**(1): p. 49-64.
15. W. Zhou, D. Loney, F.L. Degertekin, D.W. Rosen, and A.G. Fedorov, *What controls dynamics of droplet shape evolution upon impingement on a solid surface?* AIChE Journal, 2013: p. n/a-n/a.
16. L. Gao and T.J. McCarthy, *Contact angle hysteresis explained.* Langmuir, 2006. **22**(14): p. 6234-6237.
17. R.E. Johnson Jr and R.H. Dettre, *Contact angle hysteresis. III. Study of an idealized heterogeneous surface.* The journal of physical chemistry, 1964. **68**(7): p. 1744-1750.
18. H. Eral and J. Oh, *Contact angle hysteresis: a review of fundamentals and applications.* Colloid and polymer science, 2013. **291**(2): p. 247-260.

19. P.D. Spelt, *A level-set approach for simulations of flows with multiple moving contact lines with hysteresis.* Journal of Computational Physics, 2005. **207**(2): p. 389-404.
20. L. Wang, H.-b. Huang, and X.-Y. Lu, *Scheme for contact angle and its hysteresis in a multiphase lattice Boltzmann method.* Physical Review E, 2013. **87**(1): p. 013301.
21. H. Kusumaatmaja and J. Yeomans, *Modeling contact angle hysteresis on chemically patterned and superhydrophobic surfaces.* Langmuir, 2007. **23**(11): p. 6019-6032.
22. Š. Šikalo, H.-D. Wilhelm, I. Roisman, S. Jakirlić, and C. Tropea, *Dynamic contact angle of spreading droplets: Experiments and simulations.* Physics of Fluids (1994-present), 2005. **17**(6): p. 062103.
23. X. He, S. Chen, and R. Zhang, *A Lattice Boltzmann Scheme for Incompressible Multiphase Flow and Its Application in Simulation of Rayleigh–Taylor Instability.* Journal of Computational Physics, 1999. **152**(2): p. 642-663.
24. J. Latt, *Hydrodynamic limit of lattice Boltzmann equations* PhD. 2007: University of Geneva.
25. Y.-H. Qian and S.-Y. Chen, *Dissipative and dispersive behaviors of lattice-based models for hydrodynamics.* PHYSICAL REVIEW E, 2000. **61**(3): p. 2712-2716.
26. D. Kwok, T. Gietzelt, K. Grundke, H.-J. Jacobasch, and A.W. Neumann, *Contact angle measurements and contact angle interpretation. 1. Contact angle measurements by axisymmetric drop shape analysis and a goniometer sessile drop technique.* Langmuir, 1997. **13**(10): p. 2880-2894.
27. B. Bezuglyi, O. Tarasov, and A. Fedorets, *Modified tilting-plate method for measuring contact angles.* Colloid Journal, 2001. **63**(6): p. 668-674.
28. O.N. Tretinnikov and Y. Ikada, *Dynamic wetting and contact angle hysteresis of polymer surfaces studied with the modified Wilhelmy balance method.* Langmuir, 1994. **10**(5): p. 1606-1614.
29. A.J. Briant, A.J. Wagner, and J.M. Yeomans, *Lattice Boltzmann simulations of contact line motion. I. Liquid-gas systems.* PHYSICAL REVIEW E, 2004. **69**(3): p. 031602.
30. T. Lee and L. Liu, *Lattice Boltzmann simulations of micron-scale drop impact on dry surfaces.* Journal of Computational Physics, 2010. **229**(20): p. 8045-8063.
31. H. Ding and P.D.M. Spelt, *Wetting condition in diffuse interface simulations of contact line motion.* PHYSICAL REVIEW E, 2007. **75**(4): p. 046708.
32. W. Zhou, D. Loney, A.G. Fedorov, F.L. Degertekin, D.W. Rosen, R.I. Campbell, and D. Bourell, *Shape evolution of multiple interacting droplets in inkjet deposition.* Rapid Prototyping Journal, 2015. **21**(4).
33. D.B. Soltman, *Understanding inkjet printed pattern generation* 2011: University of California, Berkeley.